

Honoring the 133rd anniversary of the Mach Zehnder interferometer *

J. Heldens^{a,1}, The UBCx Phot1xSilicon Photonics Design, Fabrication and Data Analysis course team¹

^a*No affiliation for the purpose of this article, Our house, in the middle of our street, in our home town, The Netherlands*

Abstract

To honor the 133rd anniversary of the Mach Zehnder interferometer, 5 integrated Mach Zehnder interferometers are fabricated using e-beam lithography in a Silicon on Insulator platform. The theory behind the transfer function of the Mach Zehnder interferometer is treated followed by the modeling of the integrated Mach Zehnder interferometer using ANSYS Lumerical Mode and Interconnect. A corner analysis is performed to predict the range within which the values for the free spectral range, group index and effective index of the fabricated device will fall. Subsequently the devices are fabricated at the Applied Nano Tools facility and measured by the staff of the University of British Columbia. The measured transmission spectra are analyses and compared to the simulation data.

Keywords: SOI, photonics, Mach Zehnder interferometer

1. Introduction

It has been 133 years since Ludwig Mach and Ludwig Zehnder published their seminal papers Mach [1], Zehnder [2] on what would become known as the Mach Zehnder interferometer. An improvement on the Jamin interferometer Jamin [3], the Mach Zehnder interferometer (**MZI**) has been used in a variety of fields to detect any thing that can cause an optical change to one of its arms. In recent years its application field has been widened as it has found application as a optical switch in integrated optics. To celebrated this mile stone we shall first reiterate the theory behind the MZI based on the a simple plane wave free-space beam-splitter model. Then we will model 5 unbalanced integrated MZIs on a Silicon on Insulator (**SOI**) platform which will be subsequently fabricated using E-beam lithography (**EBL**) at the Applied Nano Tools (**ANT**) facility.

*This document is only intended as a report for the course and not fit for any other purpose.
Email address: Jeroen@email.com (J. Heldens)

After fabrication the free sprectal range (**FSR**) of the MZIs will be measured and compared to the theory.

2. Theory

In this report we will used a simple plane wave free-space beam-splitter model for the MZI as described in the book Silicon Photonics Design Chrostowski and Hochberg [4]. This model is valid for single mode waveguides, only considering the field intensity inside the waveguide and ignoring other contributions. Assuming that the waveguides in both arms only differ in length, we take I_i to be the input intensity. Describing the waveguide propagation with $\beta = 2\pi n \lambda^{-1}$, we arrive at the following equation for the MZI output intensity I_0 :

$$I_0 = \frac{I_i}{4} |e^{-i\beta L_1 - \frac{\alpha}{2} L_1} + e^{-i\beta L_2 - \frac{\alpha}{2} L_2}|^2 \quad (1)$$

Where L_1 and L_2 are the lengths of the respective waveguides in the interferometer arms and α is the waveguide propagation loss. Assuming α to be zero and $L_1 \neq L_2$ Equation 1simplifies to:

$$I_0(\lambda) = \frac{I_i}{2} = [1 + \cos(-\beta(\lambda)\Delta_{L_1-L_2})] \quad (2)$$

We will use Equation 2 as the transfer function for the MZI. Equation 2 provides us with a periodically varying signal whose period is called the free spectral range (**FSR**) of the MZI. An expression for the FSR in the form of $\Delta\lambda$ can be obtained by realizing that $\Delta\beta$ between two peaks must be equal to $2\pi/\Delta L$. If we now approximate β to vary linearly with λ we can arrive at the following equation for the FSR:

$$FSR = \Delta\lambda = \frac{\lambda^2}{n_g \Delta_{L_1-L_2}} \quad (3)$$

We can determine the FSR by measuring the distance between two peaks in the transmission spectrum, around the wavelength of interest. Equation 3 then provides us access to the group index n_g

3. Modeling and simulation

In preparation of the experimental results we will model the standard ANT SOI strip waveguides in ANSYS Lumerical MODE. Further, with help of the standard models from the SiEPIC_EBeam_PDK Chrostowski et al. [5] we will perform circuit simulations on the 5 MZI's that will be fabricated with different values for $\Delta_{L_1-L_2}$.

Parameter	Value	Unit
Core width	500	nm
Core height	200	nm
Central wavelength	1550	nm
Wavelength span	50	nm
Refractive index Si	Si Palik Palik [6]	-
Refractive index SiO ₂	SiO ₂ Palik Palik [6]	-
Polarization	TE	-

Table 1: ANT SOI strip waveguide model parameters

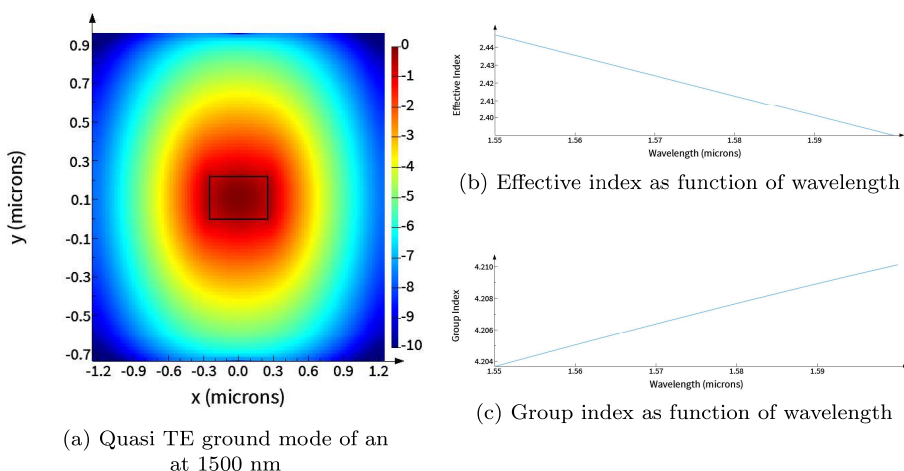


Figure 1: TE ground mode, Effective index and Group Index of the 500x220 nm SIO waveguide used in this report

Reference	ΔL_1-L_2 [μm]	Expected FSR [nm]
MZI_1	100	5.67
MZI_2	200	2.85
MZI_3	300	1.90
MZI_4	900	0.6
MZI_5	1900	0.3

Table 2: Simulated Free spectra ranges for MZIs with path length difference between 100 μm and 1900 μm

3.1. Waveguide modeling

We will model the standard ANT SOI strip waveguide with the following parameters: Modeling this waveguide we find a quasi (98%) TE ground mode with a profile as depicted in Based on these simulation results, we find a compact model for this waveguide by performing a Taylor expansion around the central wavelength:

$$n_{eff}(\lambda) = n_1 + n_2(\lambda - \lambda_0) + n_3(\lambda - \lambda_0)^2 \quad (4)$$

By fitting the simulation data we arrive at $n_1 = 2.44682$, $n_2 = -1.3339$, $n_3 = -0.0439366$ and $\lambda_0 = 1550$ nm.

3.2. Simulation

Using ANSYS Lumerical interconnect we create a circuit incorporating two grating couplers, two y-splitter and one waveguide of length 100 μm and the other of length 100 μm + ΔL_1-L_2 . Varying ΔL_1-L_2 according to Table (FSR interconect) we find the FSR in the last column of Table 2 and the transmission spectra for MZI_1 and MZI_5 in Figure 4.

3.3. Manufacturing Challenges

One of the main benefits of modern lithographic technologies such as EBL is the ability to almost exactly reproduce the same circuit in astonishing quantities. This has been the foundation under the IT revolution that has brought us the powerful computers that we have all grown so accustomed to. The crux, however, is in the almost. Where Mach and Zehnder could, or rather had to, tweak each individual interferometer to operate as they specified, in integrated optics we have to deal with process variations. Each repeated process, no matter how well controlled, will have certain variation. This can be variation in the quality of the used materials, variation in the settings of the devices or any other variation in the parameters of the process. Because tuning the process at every iteration would defeat the purpose, we end up with circuits that are slightly different from each other. To cope with this, the process is adjusted not to produce the circuit exactly as designed but rather to produce an acceptable small amount of variation. In turn the design can then be adjusted to have the



Figure 2: Transmission spectrum of a MZI's with $\Delta L_1 - L_2 = 100 \mu\text{m}$ (green line) and $1900 \mu\text{m}$ (blue line)

manufactured circuit come as close as possible to the intended design. To do this the effects of the process variations have to be investigated.

The main component in our design of the MZI is the waveguide, as such it makes sense to investigate the impact of process variations on the waveguide properties. The properties of the waveguide are defined by its refractive index, its height and width. The first two are determined by the used wafer. The refractive index variation of a Si wafer is small compared to the variation in height of the Si layer, so we will account for the latter. The width of the waveguide is controlled by the lithograph process and suffers variations from the both the patterning and the etching processes, as such, this is a good second parameter to simulate. Instead of looking at the effect of variations in width and height separately we will perform a corner analysis. This type of analysis looks at the combinations of maximum and minimum expected values for the considered parameters. In the parameter space these combinations are given by the corners of a rectangle hence the name. The benefit of a corner analysis over a standard analysis is that a corner analysis also takes in to account possible interactions between the tested variables.

Corner	Width [nm]	Height [nm]
NM	500	220
RT	470	223.1
RB	470	215.3
LT	510	223.1
LB	510	215.3

Table 3: Corner values of the corner analysis: nominal (NM), Right Top (RT), Right Bottom (RB), Left Top (LT), Left Bottom (LB)

The nominal dimensions of our waveguide are, as given above, 500 nm x 220 nm. The waveguide width is assumed to vary between 470 nm and 510 nm and its height is assumed to vary between 215.3 and 223.1 nm. With these data we find the corners of our analysis as given in Table (3). Modeling the waveguide for the four

	Effective index	Corner		Group index	Corner
Max	2.47	LT	Max	4.24	RT
Min	2.37	RB	Min	4.16	LB
(a) Effective index range			(b) Group index range		

Table 4: Ranges for Effective and Group index found from the corner analysis

Reference	ΔL_1-L_2 [μm]	NM	RT	RB	LT	LB
MZI_1	100	5,68E+06	5,68E+06	5,64E+06	5,76E+06	5,76E+06
MZI_2	200	2,88E+06	2,84E+07	2,84E+07	2,88E+06	2,88E+06
MZI_3	300	1,88E+06	1,92E+07	1,88E+06	1,92E+07	1,92E+07
MZI_4	900	6,40E+05	6,40E+05	6,00E+04	6,40E+05	6,40E+05
MZI_5	1900	3,20E+05	2,80E+05	3,20E+05	2,80E+05	2,80E+05

Table 5: Free Spectral ranges for the designed MZIs at the nominal design and corners of the corner analysis

corners of the corner analysis we arrive at four additional compact models for the waveguides of our MZI.

If we simulate our MZI circuit in ANSYS Lumerical interconnect based on these additional compact models we find ranges for the Effective index, the Group index and the FSR (see tables 4and 5) . We expect the measured values for the manufactured design to fall with in these ranges. If for any reason a value within this range would not meet our design requirements, we would have to either redesign the circuit in such a way that the ranges shift to acceptable values or accept that not all manufactured devices will meet the design requirements. An other approach, common in the semiconductor industry, is to relax the requirements for the devices that do not meet the requirements and sell them as a separate product this is called chip binning Intel Corporation [7].

4. Design and Manufacturing

4.1. Design

To design our MZI's we made use of the Klayout design software Köfferlein [8] in combination with the SiEPIC_EBeam_PDK Chrostowski et al. [5]. Using this software the design process is mainly one of picking and placing the correct components. In this way 5 MZIs and 1 loopback structure were designed. Figure 3 gives the design of MZA1a as an example. As the figure shows, the design consists of two grating couplers, two y splitters and two stretches of waveguide with a length difference of in this case 100 μm .

4.2. Manufacturing

The photonic devices were fabricated using the NanoSOI MPW fabrication process by Applied Nanotools Inc. (<http://www.appliednt.com/nanosoi>; Edmonton, Canada) which is based on direct-write 100 keV electron beam lithography technology. Silicon-on-insulator wafers of 200 mm diameter, 220 nm device thickness and 2 μ m buffer oxide thickness are used as the base material for the fabrication. The wafer was pre-diced into square substrates with dimensions of 25x25 mm, and lines were scribed into the substrate backsides to facilitate easy separation into smaller chips once fabrication was complete. After an initial wafer clean using piranha solution (3:1 H₂SO₄:H₂O₂) for 15 minutes and water/IPA rinse, hydrogen silsesquioxane (HSQ) resist was spin-coated onto the substrate and heated to evaporate the solvent. The photonic devices were patterned using a JEOL JBX-8100FS electron beam instrument at The University of British Columbia. The exposure dosage of the design was corrected for proximity effects that result from the backscatter of electrons from exposure of nearby features. Shape writing order was optimized for efficient patterning and minimal beam drift. After the e-beam exposure and subsequent development with a tetramethylammonium sulfate (TMAH) solution, the devices were inspected optically for residues and/or defects. The chips were then mounted on a 4" handle wafer and underwent an anisotropic ICP-RIE etch process using chlorine after qualification of the etch rate. The resist was removed from the surface of the devices using a 10:1 buffer oxide wet etch, and the devices were inspected using a scanning electron microscope (SEM) to verify patterning and etch quality. A 2.2 μ m oxide cladding was deposited using a plasma-enhanced chemical vapour deposition (PECVD) process based on tetraethyl orthosilicate (TEOS) at 300°C. Reflectometry measurements were performed throughout the process to verify the device layer, buffer oxide and cladding thicknesses before delivery.

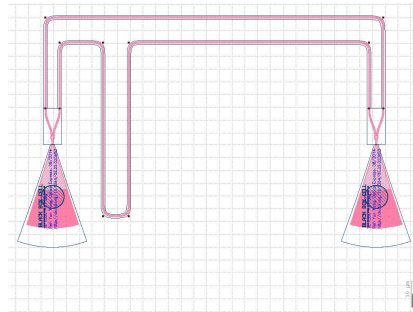


Figure 3: Layout of MZI1a

5. Measurements and Analysis

The analysis of the manufactured structured has been performed in two steps. In the first step the structures were measured by the UBC using their automated measuring setup. These measurements are detailed in the measurement section below. After the measurements were completed the obtained data was analyzed using matlab scripts translated in to python code. The results of this analysis can be found in the section analysis.

Reference	$\Delta L1-L2$ [μm]	FSR [nm]	Est. N_g	Calc. N_g	Calc. N_{eff}
MZI1a	100	5.77	4.18	4.21	2.39
MZI2a	200	2.86	4.20	4.22	2.40
MZI3a	300	1.93	4.19	4.22	2.40
MZI4a	900	0.64	4.19	4.21	2.40
MZI5a	1900	0.30	4.18	4.22	2.40

Table 6: Analysis data of the manufactured MZIs

5.1. Measurements

To characterize the devices, a custom-built automated test setup Chrostowski and Hochberg [9], Maple Leaf Photonics [10]with automated control software written in Python was used Caverley [11]. An Agilent 81600B tunable laser was used as the input source and Agilent 81635A optical power sensors as the output detectors. The wavelength was swept from 1500 to 1600 nm in 10 pm steps. A polarization maintaining (PM) fibre was used to maintain the polarization state of the light, to couple the TE polarization into the grating couplers Wang et al. [12]. A 90° rotation was used to inject light into the TM grating couplers Wang et al. [12]. A polarization maintaining fibre array was used to couple light in/out of the chipPLC Connections [13].

5.2. Analysis

To start the analysis of the data the transmission spectrum is first cleaned. This is mainly done by background correcting the transmission spectrum by subtracting a fourth order polynomial from the the data. This approach effectively removes the influence of the wavelength dependence of the grating couplers from the transmission spectrum. further more any infinitely negative peaks are replaced by a value of -50 dB and the spectrum is de-noised using a moving average. Subsequently the distance between the peaks of the transmission spectrum are identified giving us the first results in the form of the FSR and the estimated Group index (Est. N_g) see Table 6 which is calculated from the FSR using equation 3. Subsequently the MZI transfer function is fitted to the measurement data using as 2.4 as an initial guess for n_1 , obtaining n_2 from the relation $n_g = n_1 - n_2\lambda$ and using a fit to the slope of the group index to obtain the dispersion to find n_3 to via the relation $Dispersion = -\frac{\lambda}{c}2n_3$. From the fitted transfer function we find the values for n_1 , n_2 and n_3 which allow us to calculate the group index (Calc. N_g) and the effective index (Calc. N_{eff}) in Table 6.

6. Conclusions

Comparing the values for the group index and the effective index from table 6 to the values found during the corner analysis in table 4we find that the experimental values are well within the simulated ranges. For the FSR we find

that the experimental FSRs are somewhat above the FSR ranges found in table 5. Comparing the nominal values from table 5 to the nominal values from table 2 it seems that something might have gone wrong during the calculation of the FSR in table 5. This would normally warrant further investigation, but this is however beyond the scope of this report.

7. Acknowledgment

We acknowledge the edX UBCx Phot1x Silicon Photonics Design, Fabrication and Data Analysis course, which is supported by the Natural Sciences and Engineering Research Council of Canada (NSERC) Silicon Electronic-Photonic Integrated Circuits (SiEPIC) Program. The devices were fabricated by Cameron Horvath at Applied Nanotools, Inc. Omid Esmaeeli performed the measurements at The University of British Columbia. We acknowledge Lumerical Solutions, Inc., Mathworks, Python, and KLayout for the design software.

References

- [1] L. Mach, Über einen interferenzrefraktor, Zeitschrift für Instrumentenkunde (1892) 89–93.
- [2] L. Zehnder, Ein neuer interferenzrefraktor, Zeitschrift für Instrumentenkunde (1891) 275–285.
- [3] Jamin, Neuer interferential-refractor, Annalen der Physik 174 (1856) 345–349. URL: <https://onlinelibrary.wiley.com/doi/abs/10.1002/andp.18561740619>. doi:<https://doi.org/10.1002/andp.18561740619>. arXiv:<https://onlinelibrary.wiley.com/doi/pdf/10.1002/andp.18561740619>.
- [4] L. Chrostowski, M. Hochberg, Silicon Photonics Design: From Devices to Systems, Cambridge University Press, 2015.
- [5] L. Chrostowski, Z. Lu, J. Flueckiger, X. Wang, J. Klein, A. Liu, J. Jhoja, J. Pond, Design and simulation of silicon photonic schematics and layouts, in: L. Vivien, L. Pavesi, S. Pelli (Eds.), Silicon Photonics and Photonic Integrated Circuits V, volume 9891, International Society for Optics and Photonics, SPIE, 2016, p. 989114. URL: <https://doi.org/10.1117/12.2230376>. doi:10.1117/12.2230376.
- [6] E. D. Palik, Handbook of Optical Constants of Solids, Academic Press, 1985.
- [7] Intel Corporation, From Sand to Silicon: The Making of a Chip (32nm Version), https://download.intel.com/newsroom/kits/chipmaking/pdfs/Sand-to-Silicon_32nm-Version.pdf, 2009. Accessed: 2025-11-29.

- [8] M. Köfferlein, Klayout: Layout viewer and editor, <https://www.klayout.de/>, 2025. Accessed: 2025-11-29.
- [9] L. Chrostowski, M. Hochberg, Silicon Photonics Design: From Devices to Systems, 2015. doi:10.1017/cbo9781316084168.
- [10] Maple Leaf Photonics, Maple leaf photonics, <http://mapleleafphotonics.com>, 2025. Accessed: November 27, 2025.
- [11] M. Caverley, Siepic probe station python code, <http://siepic.ubc.ca/probestation>, 2025. Developed using Python code by Michael Caverley. Accessed: November 27, 2025.
- [12] Y. Wang, X. Wang, J. Flueckiger, H. Yun, W. Shi, R. Bojko, N. A. F. Jaeger, L. Chrostowski, Focusing sub-wavelength grating couplers with low back reflections for rapid prototyping of silicon photonic circuits, Optics Express 22 (2014) 20652–20662. doi:10.1364/OE.22.020652.
- [13] PLC Connections, Plc connections, <http://www.plcconnections.com>, 2025. Accessed: November 27, 2025.